One-dimensional fluid diffusion induced by constant-rate flow injection: Theoretical analysis and application to the determination of fluid permeability and specific storage of a cored rock sample

One-dimensional fluid diffusion induced by constant-rate flow injection: Theoretical analysis and application to the determination of fluid permeability and specific storage of a cored rock sample

I. Song,[1] S. C. Elphick, I. G. Main, B. T. Ngwenya, and N. W. Odling
School of Geosciences, University of Edinburgh, Edinburgh, UK

N. F. Smyth
School of Mathematics, University of Edinburgh, Edinburgh, UK

Received 8 January 2003; revised 2 February 2004; accepted 23 February 2004; published 13 May 2004.

[1] We describe the conceptual design and first application of a new method for simultaneously measuring the fluid permeability and specific storage of a rock sample. In our laboratory tests, a constant flow rate single-stroke piston pump injects fluid into a cored rock specimen placed between two reservoirs in which fluid pressure is recorded. For this geometry we have derived a new analytic solution of the governing diffusion equation describing the one-dimensional fluid flow. This new analytic solution in the time domain consists of two parts: an asymptotic linear function of time, and a transient part which decays to zero as time increases. The model predicts that the fluid pressures of the upstream and downstream reservoirs both increase linearly with time after the initial transient vanishes. The slope of the linear pressure variation depends on the specific storage of the rock sample for a given test condition, and the differential pressure between the two reservoirs is related to the permeability. If the downstream pressure is not recorded, the permeability can be calculated from the zero intercept of the linear upstream fluid pressure variation. This calculation is quite straightforward and no tedious history curve matching is required. We applied our new method to measure fluid permeability and specific storage of Westerly granite. The measured values of the permeability are consistent with those published in the literature. The main advantages of our method are the reliability of the testing method, its economy of time, and the flexibility in adapting the system parameters to tests at different conditions. *INDEX TERMS:* 1829 Hydrology: Groundwater hydrology; 1832 Hydrology: Groundwater transport; 3994 Mineral Physics: Instruments and techniques; *KEYWORDS:* fluid diffusion, fluid permeability, specific storage, hydraulic properties, Westerly granite

Citation: Song, I., S. C. Elphick, I. G. Main, B. T. Ngwenya, N. W. Odling, and N. F. Smyth (2004), One-dimensional fluid diffusion induced by constant-rate flow injection: Theoretical analysis and application to the determination of fluid permeability and specific storage of a cored rock sample, *J. Geophys. Res.*, *109*, B05207, doi:10.1029/2003JB002395.

1. Introduction

[2] Characterization of the hydraulic properties of rocks is essential in the exploitation of natural fluid resources, such as water, steam, petroleum, and natural gas, buried underground. The low permeability of tight rocks is often exploited for retarding the underground movement of hazardous wastes [*Roxburgh*, 1987; *Savage*, 1995]. In conjunction with the physical properties of reservoir rocks, the hydraulic characteristics of the fluid trapped within the pore space influence the elastic response [*Biot*, 1941; *Rice and Cleary*, 1976; *Detournay and Cheng*, 1988], the inelastic behavior [*Wong and Biegel*, 1985; *Fournier*, 1996; *Simpson*, 2001; *Simpson et al.*, 2001], and the time-dependent reactions [*Johnson et al.*, 1973; *Mortensen et al.*, 1977; *Roeloffs et al.*, 1989] of rocks. Therefore reliable measurements of the hydraulic flow parameters of rocks are essential for modeling of many geologic processes, for the prediction of seismic sensitivity, and for the design of aquitard systems for safe storage of hazardous wastes.

[3] In general, the nature of fluids in reservoir rocks can be characterized in terms of quantity (concentration) and mobility of the fluid. The specific storage S_s deals with the capacity of a reservoir rock for storing a fluid as a function of fluid pressure, while the permeability k measures

[1]Now at Institute for Geology, Mineralogy, and Geophysics, Ruhr-University Bochum, Bochum, Germany.

0148-0227/04/2003JB002395$09.00

the ability of the rock to transmit a fluid through the interconnected passages and voids of the rock. Because saturated rock comprises a solid matrix with fluid distributed throughout in connected pore spaces, the compressive storage of fluid in the rock can be obtained from the compressibility of each part and the connected porosity of the rock sample [*Brace et al.*, 1968]. According to Darcy's law, permeability can be determined in steady state flow conditions by the linear relationship between the total fluid flux across a sample, and the measured pressure gradient developed along the specimen. However this method is not always convenient for extremely low permeability rocks because long periods of time are required to establish a steady state [*Hsieh et al.*, 1981; *Zeynaly-Andabily and Rahman*, 1995].

[4] In order to achieve results more rapidly, a non-steady state method known as the pulse transient method was suggested by *Brace et al.* [1968]. The pulse method is relatively fast, and has been widely adopted to measure the permeability of tight rocks, with slight modifications [e.g., *Zoback and Byerlee*, 1975; *Trimmer et al.*, 1980; *Neuzil et al.*, 1981; *Lin*, 1982; *Lin et al.*, 1986; *Zeynaly-Andabily and Rahman*, 1995; *Liang et al.*, 2001; *Kwon et al.*, 2001]. The experimental configuration consists of a cylindrical specimen held between two fluid reservoirs. A sudden pulse in the fluid pressure in the upstream reservoir induces fluid flow across the specimen due to the pressure difference between the two reservoirs. The pressure difference decay rate is related to the permeability of the sample. *Brace et al.* [1968] presented an approximate solution for fluid permeability under the assumption that the specific storage of the rock specimen is negligible. This simplification is no longer needed when numerical methods are used [*Trimmer et al.*, 1980; *Lin et al.*, 1986]. However, it is still necessary to measure the specific storage of the sample independently. *Hsieh et al.* [1981] derived an exact analytical solution for the calculation of both the specific storage and the permeability. However calculating these two unknowns requires a two-test procedure with different size reservoirs [*Neuzil et al.*, 1981] or a history matching routine to compare experimental data with theoretical curves [*Zeynaly-Andabily and Rahman*, 1995].

[5] If a fluid is pumped at a constant flow rate into one end of a cylindrical rock specimen, the pressure in the pump (or upstream reservoir) increases with time. The pressure difference along the sample itself eventually stabilizes to a constant value when the downstream flow rate equals the injection flow rate. The permeability of the sample can be calculated from this stabilized, steady state pressure difference using Darcy's law. However, it may take a relatively long time to reach this steady state flow for rocks with very low permeability [*Olsen et al.*, 1985; *Esaki et al.*, 1996]. *Morin and Olsen* [1987] presented an analytic method for determining values of the specific storage and permeability from the initial transient response during the early testing time. *Esaki et al.* [1996] improved this method by taking into account the compressive storage of the flow pump system. However, this method also requires a tedious curve-matching routine.

[6] This paper presents a new technique for simultaneously measuring permeability and specific storage of a single core sample, based on the theoretical analysis of the one-dimensional fluid diffusion induced by a constant-rate flow pump into a specimen placed between two reservoirs (Figure 1). In the conceptual model, the downstream reservoir is sealed, and a pump in the upstream reservoir forces fluid through the rock at a constant flow rate. Our analytic solution of the pressure diffusion equation with this boundary condition provides a new method of simultaneously determining the permeability and the specific storage of a rock sample in a straightforward, reliable and relatively rapid way. We validated the method by applying it to Westerly granite, which has been commonly used as a standard rock type for hydraulic and mechanical rock properties.

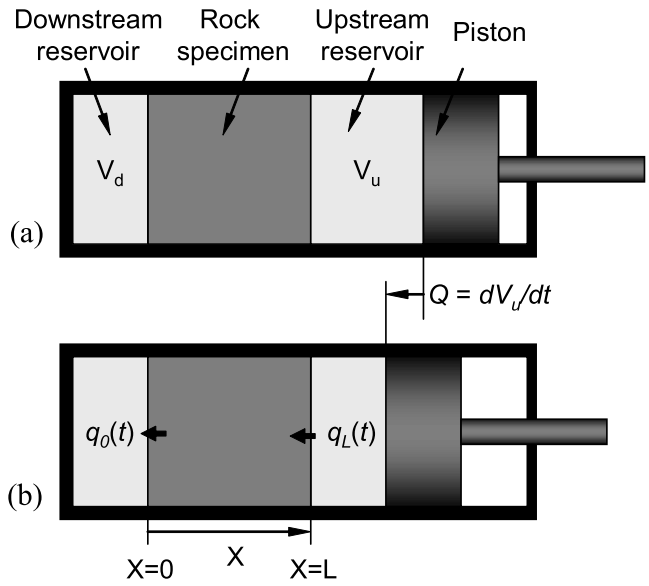

Figure 1. Schematic diagram of the test system. (a) A specimen located between two reservoirs with an initially equilibrated fluid pressure in the closed system, and (b) the fluid compression by the piston stroke inducing one-dimensional diffusion along the specimen. Q is the pumping rate defined by the piston speed and the piston area; $q_0(t)$ and $q_L(t)$ are the flow rate at the specimen boundaries, $x = 0$ and L, respectively.

2. Governing Equation and Initial-Boundary Conditions

[7] The schematic diagram and the boundary conditions are depicted in Figure 1. The experimental arrangement consists of a cylindrical rock specimen placed between two reservoirs with a flow pump connected to the upstream reservoir. For the boundary condition at $x = L$, *Morin and Olsen* [1987] assumed that the flow induced by the pressure pump penetrates immediately into the rock specimen. If the pressure in the pump system increases, however, this assumption is no longer valid because the upstream reservoir is deformable and the fluid is compressible. Thus the actual flow rate entering the specimen at a certain time t equals the difference between the total pumping rate and the extra volume change induced by the compliance of the pump system and the compressibility of the fluid per unit

time interval. Thus the actual flow rate $q_L(t)$ at $x = L$ can be written as follows [*Esaki et al.*, 1996]:

$$q_L(t) = Q - S_u \frac{dp_u}{dt}, \tag{1}$$

where Q, S_u and p_u are the constant pumping rate, the compressive storage of the upstream reservoir and the upstream pressure, respectively.

[8] The inlet fluid migrates through the interconnected voids in the rock to the other side of the specimen (Figure 1b). The downstream reservoir is closed, so the downstream fluid pressure increases. The relationship between the flow rate $q_0(t)$ at $x = 0$ and the rate of change of the pressure dp_d/dt is expressed as

$$q_0(t) = S_d \frac{dp_d}{dt}, \tag{2}$$

where S_d and p_d are the compressive storage and the fluid pressure of the downstream reservoir, respectively.

[9] Both S_u and S_d are adjustable in laboratory tests by changing the volumes of the upstream and downstream reservoirs V_u and V_d, respectively. For example, if the downstream volume V_d is zero, S_d vanishes and $q_0(t) = 0$. The upstream reservoir volume V_u can be easily adjusted by changing the position of the piston (Figure 1a). Our new boundary condition is more general than that taken by *Morin and Olsen* [1987] or *Esaki et al.* [1996] because the constant downstream pressure ($dp_d/dt = 0$) boundary condition they used is a special case corresponding to $S_d \rightarrow \infty$ in our test arrangement.

[10] The fluid pore pressure p as a function of time t and axial distance x is described by the diffusion equation

$$\frac{\partial^2 p(x,t)}{\partial x^2} - \frac{1}{\alpha}\frac{\partial p(x,t)}{\partial t} = 0, \tag{3}$$

where α is the hydraulic diffusivity expressed as $k/\mu S_s$, with μ the dynamic viscosity of the fluid. The initial condition ($t = 0$) is given by

$$p(x,0) = 0, \qquad 0 \le x \le L \tag{4}$$

and the boundary conditions at $x = 0$ and $x = L$ are

$$x = 0 : \frac{S_d}{KA}\frac{dp_d}{dt} - \left(\frac{\partial p}{\partial x}\right)_{x=0} = 0, \qquad t > 0 \tag{5}$$

$$x = L : \frac{S_u}{KA}\frac{dp_u}{dt} + \left(\frac{\partial p}{\partial x}\right)_{x=L} = \frac{Q}{KA}, \qquad t > 0, \tag{6}$$

where $K = k/\mu$ and the other parameters are

- $p(x, t)$ fluid pressure in the sample as a function of x and t;
- p_d fluid pressure at the downstream reservoir;
- p_u fluid pressure at the upstream reservoir;
- x distance from the downstream boundary along the sample;
- t time from the start of pumping;
- A cross-sectional area of the sample;
- L length of the sample;
- k permeability of the sample;
- μ dynamic viscosity;
- S_s specific storage of the sample;
- S_u upstream compressive storage;
- S_d downstream compressive storage.

3. Theoretical Analysis

3.1. Analytic Solution

[11] The partial differential equation (3) with the initial-boundary values given by equations (4), (5) and (6) was solved by the Laplace transform method. The detailed procedure is given in Appendix A. The solution for fluid pressure as a function of position x and time t is

$$p(x,t) = \frac{F}{\beta}\left(t + \frac{x^2}{2\alpha} + \lambda_d x - \frac{L^3}{6\alpha^2\beta} - \frac{\lambda_u + \lambda_d}{2\alpha\beta}L^2 - \frac{\lambda_u\lambda_d}{\beta}L\right) - 2F\sum_{m=1}^{\infty}\frac{\exp\left(-\alpha\phi_m^2 t\right)(\cos\phi_m x - \alpha\lambda_d\phi_m\sin\phi_m x)}{\phi_m a\sin\phi_m L + \phi_m^2 b\cos\phi_m L} \tag{7}$$

where $\lambda_u = \frac{S_u}{KA}$, $\lambda_d = \frac{S_d}{KA}$, $F = \frac{Q}{KA}$, $\beta = \frac{L}{\alpha} + \frac{S_u}{KA} + \frac{S_d}{KA}$, $a = 3 - 5\lambda_u\lambda_d\alpha^2\phi_m^2 - \alpha L(\lambda_u + \lambda_d)\phi_m^2$, and $b = L + 4\alpha(\lambda_u + \lambda_d) - \lambda_u\lambda_d\alpha^2 L\phi_m^2$. The eigenvalues ϕ_m are the roots ϕ of

$$\tan\phi L = \frac{\alpha\phi(\lambda_u + \lambda_d)}{\lambda_u\lambda_d\alpha^2\phi^2 - 1}. \tag{8}$$

The analytic solution consists of a steady state part (asymptotic solution) and a transient part (series solution). At the beginning of pumping, the transient dominates, but then decays with time because of the negative exponential term in equation (7) and eventually becomes negligible. In a real test, we can measure the fluid pressures only at the upstream and downstream reservoirs. The pressures at the upstream and downstream reservoirs as a function of time can be found by setting $x = 0$ and $x = L$ in equation (7), giving

$$p_u(t) = \frac{F}{\beta}\left(t - \frac{L^3}{6\alpha^2\beta} - \frac{\lambda_u + \lambda_d - \beta}{2\alpha\beta}L^2 - \frac{\lambda_u\lambda_d - \beta\lambda_d}{\beta}L\right) - 2F\sum_{m=1}^{\infty}\frac{\exp\left(-\alpha\phi_m^2 t\right)(\cos\phi_m L - \alpha\lambda_d\phi_m\sin\phi_m L)}{\phi_m a\sin\phi_m L + \phi_m^2 b\cos\phi_m L} \tag{9}$$

and

$$p_d(t) = \frac{F}{\beta}\left(t - \frac{L^3}{6\alpha^2\beta} - \frac{\lambda_u + \lambda_d}{2\alpha\beta}L^2 - \frac{\lambda_u\lambda_d}{\beta}L\right) - 2F\sum_{m=1}^{\infty}\frac{\exp\left(-\alpha\phi_m^2 t\right)}{\phi_m a\sin\phi_m L + \phi_m^2 b\cos\phi_m L}. \tag{10}$$

3.2. Special Cases

3.2.1. Infinite Downstream Reservoir

[12] If the downstream pressure is kept constant, for example by allowing fluid to exit the reservoirs, then the compressive storage of the downstream reservoir is effectively infinite according to equation (2). If there is no compressive storage in the upstream reservoir, the flow rate Q generated by the piston stroke is equal to the inlet flow

rate into the sample $q_L(t)$ at the upper boundary of the rock specimen (equation 1). These boundary conditions have already been used for the solution of the heat equation by *Carslaw and Jaeger* [1959, p. 113] and for the measurement of hydraulic properties in a conventional triaxial system [*Olsen et al.*, 1985; *Morin and Olsen*, 1987]. Setting $S_d = \infty$ and $S_u = 0$ simplifies the eigenvalue equation (8) to

$$\tan \phi L = \infty. \tag{11}$$

Thus ϕ_m is $(2m + 1)\pi/2L$, $m = 0, 1, 2, 3, \cdots$. Substituting these values for S_d, S_u and ϕ_m into equations (9) and (10), the upstream and downstream pressures become

$$p_u(t) = \frac{\mu QL}{kA}\left[1 - \frac{8}{\pi^2}\sum_{m=0}^{\infty}\frac{1}{(2m+1)^2}\exp\left(\frac{-\alpha(2m+1)^2\pi^2 t}{4L^2}\right)\right] \tag{12}$$

and

$$p_d(t) = 0, \tag{13}$$

respectively. Equation (12) is identical to equation (3) of the paper by *Morin and Olsen* [1987], so our generic solution reduces to the same result for this specific set of boundary conditions. In this case, a steady state is reached, since the upstream pressure p_u stabilizes at $\mu QL/kA$ after the transient term decays to a negligible value.

[13] Theoretical curves for $p_u(t)$ calculated from equation (12) are depicted in Figure 2a for two values of the specific storage for a given permeability. Both curves show an initial transient with the solution evolving asymptotically to the steady state value given by Darcy's law. The steady state fluid pressure is a function of the permeability of the rock, while the shape of the transient curve is related to the specific storage (Figure 2a). For the example with a larger specific storage (dashed line), it takes a longer time to establish a steady state flow. The permeability k can be simply calculated from the steady state pressure gradient using Darcy's law. The specific storage S_s can be determined from the initial transient curve based on graphical curve matching between experimental and theoretical data. This can also be done by a numerical method using parameter identification theory [*Esaki et al.*, 1996].

[14] When the compressive storage of the pump system (the upstream reservoir) is finite, the eigenvalue equation (8) becomes

$$\tan \phi L = \frac{1}{\alpha\lambda_u\phi}, \tag{14}$$

and the upstream fluid pressure is

$$p_u(t) = \frac{\mu QL}{kA}\left[1 - 2\sum_{m=1}^{\infty}\frac{\exp\left(-\alpha\phi_m^2 t\right)}{\phi_m^2 L\left(L + \alpha\lambda_u + \alpha^2\lambda_u^2\phi_m^2 L\right)}\right]. \tag{15}$$

Equations (14) and (15) are the same as equations (5) and (6), respectively, from *Esaki et al.* [1996]. Three theoretical curves for different S_u are shown in Figure 2b to illustrate its effect on the transient. The transient

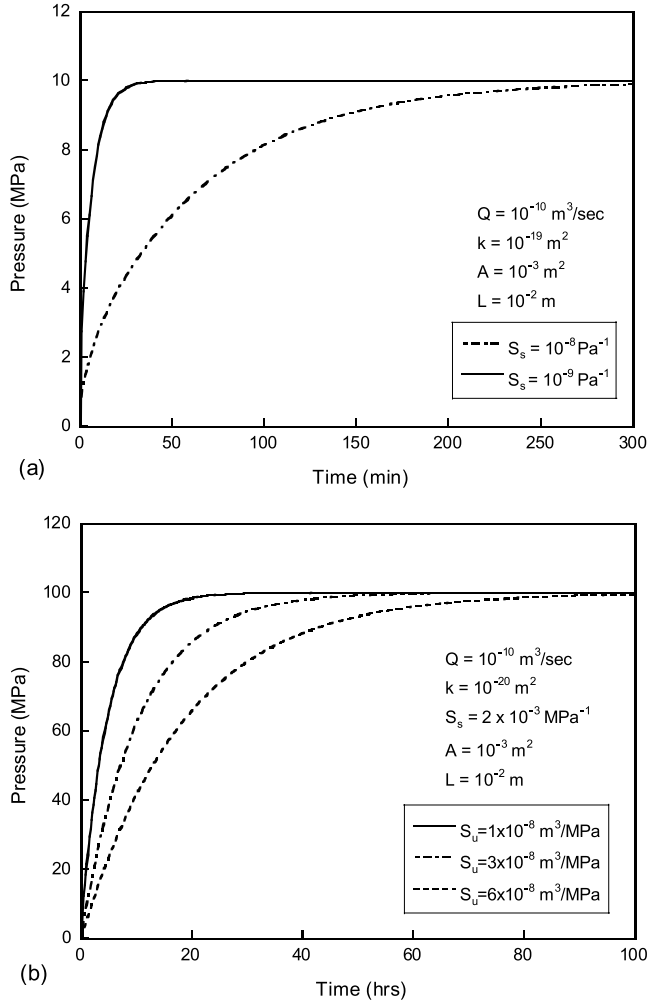

Figure 2. Theoretical curves of the upstream pressure as a function of time when the downstream pressure is zero showing the different transient curves depending on (a) the specific storages of specimen and (b) the compressive storage of upstream reservoir.

duration increases as the compliance of the system increases. While the upstream fluid pressure increases in the transient stage, the actual flow rate $q_L(t)$ at the rock boundary $x = L$ is smaller than the pumping rate Q induced by the movement of the piston according to equation (1). As the fluid flow in the rock specimen approaches the steady state, $q_L(t)$ becomes equal to Q. Thus a finite S_u does not affect the magnitude of the asymptotic maximum pressure, which is determined by the steady state flow along the specimen. The permeability can be simply calculated from Darcy's law, but it becomes more complicated to compute the specific storage of a rock specimen from the transient curve in this case.

3.2.2. Zero Downstream Reservoir

[15] If there is no downstream reservoir ($V_d = 0$), so that no fluid comes out of the specimen at the downstream side, then the compressive storage S_d of the downstream will be zero according to equation (2). To our knowledge, this boundary condition has never previously been considered in constant flow rate permeability tests, presumably because this boundary condition does not allow the fluid to pass

through the specimen. Assuming no compressive storage of the pump system, the eigenvalue equation (10) reduces to

$$\tan \phi L = 0, \tag{16}$$

so that $\phi = m\pi/L$, $m = 0, 1, 2, 3, \cdots$. The upstream and downstream pressures then reduce to

$$p_u(t) = \frac{Qt}{S_s AL} + \frac{\mu QL}{kA}\left[\frac{1}{3} - \frac{2}{\pi^2}\sum_{m=1}^{\infty}\frac{1}{m^2}\exp\left(\frac{-m^2\pi^2\alpha t}{L^2}\right)\right] \tag{17}$$

and

$$p_d(t) = \frac{Qt}{S_s AL} - \frac{\mu QL}{kA}\left[\frac{1}{6} + \frac{2}{\pi^2}\sum_{m=1}^{\infty}\frac{(-1)^m}{m^2}\exp\left(\frac{-m^2\pi^2\alpha t}{L^2}\right)\right]. \tag{18}$$

These solutions can also be found in heat conduction problems with constant flux at $x = L$ and no flux at $x = 0$, as given by *Carslaw and Jaeger* [1959, p. 112].

[16] Two examples of theoretical curves for the upstream fluid pressure as a function of time as predicted by equation (17) are depicted in Figure 3a. All parameters are the same as those for Figure 2a, for reference. Now the upstream pressure does not stabilize at a constant value. The upstream pressure increases rapidly initially, then the growth rate decreases, and the pressure asymptotically approaches a linear function. Figure 3a shows two different asymptotic slopes, dp_u/dt, for the two different specific storages S_s. However both show a common intercept, P_u^{int}, because the permeability k is the same for both curves. This indicates that the specific storage and permeability are independent and relate directly to the slope and the intercept, respectively. From equation (17), the slope and intercept of the steady state pressure curve are

$$\frac{dp_u}{dt} = \frac{Q}{S_s AL} \tag{19}$$

and

$$P_u^{\text{int}} = \frac{\mu QL}{3kA}, \tag{20}$$

where Q, A and L are known values. From equation (19), the specific storage S_s of the rock sample is inversely proportional to the slope of the linear steady state of a test record. From equation (20), the permeability k is inversely proportional to the intercept of the linear steady state upstream pressure. Another important merit of the present method with the new boundary condition is its economy of time. This can be seen from the difference between the decay times of the transients of the solutions shown in Figures 2a and 3a. According to the analysis of the transient parts of solutions (12) and (17) when $S_u = 0$, the decay duration for the latter boundary condition ($S_d \rightarrow 0$) is four times shorter than that for the former boundary condition ($S_d \rightarrow \infty$) for a given rock specimen.

[17] The method above is based solely on the measurement of upstream pressure. If we are also able to measure

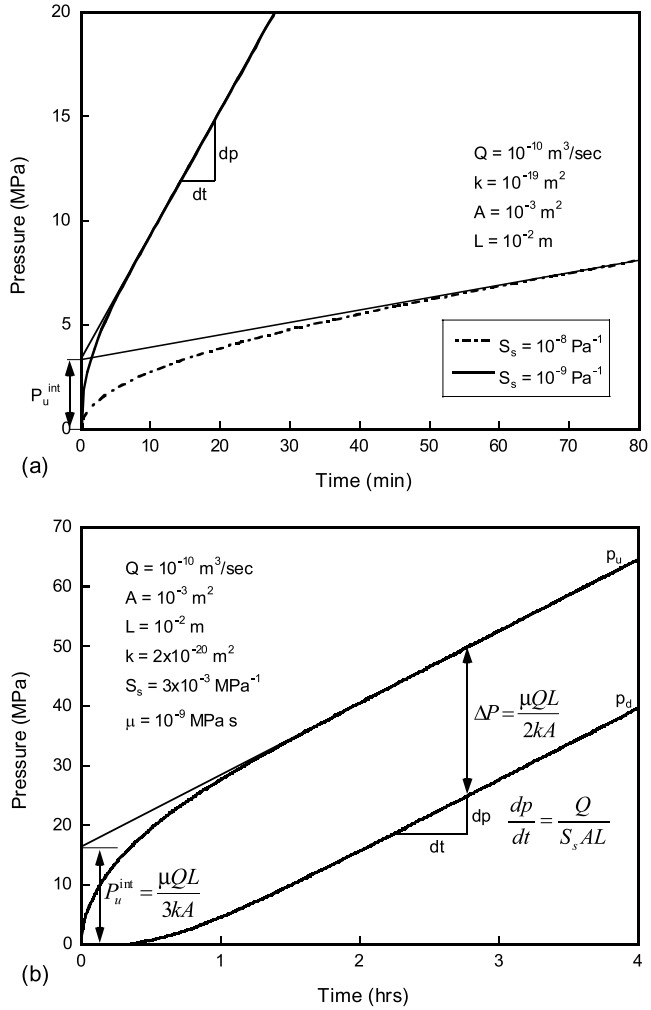

Figure 3. (a) Theoretical upstream pressures for two different specific storages as a function of time showing the linearly increasing parts after the transient stages. Note that the two intercepts are the same. (b) Theoretical pressures at both the upstream and downstream reservoirs as a function of time showing the relationship between the characteristics of the curves and hydraulic parameters of specimen. In both cases, the system compliance is neglected.

the downstream pressure, the permeability k can be simply computed by an independent method from the differential pressure ΔP between the upstream and the downstream after the transient has decayed. This pressure difference is

$$\Delta P = p_u - p_d = \frac{\mu QL}{2kA}. \tag{21}$$

The differential pressure is more reliable than the intercept, because the former is a direct measure, while the latter is an extrapolation. Obviously, the measurement of downstream pressure is very important, but would not be possible when the downstream reservoir volume is zero without using a specially designed pressure sensor. With this caveat, Figure 3b shows theoretical curves for both the upstream and downstream pressures calculated from equations (17)

and (18). The difference between the two fluid pressures, ΔP, is constant after the transient has decayed. This new boundary condition provides a simple practical method to compute the specific storage and the permeability independently on a single test, using an analysis only involving a straight line fit to the asymptote.

[18] In practical situations, however, the compressive storage of the upstream reservoir cannot be neglected because the reservoir is deformed and the fluid is compressed under increasing fluid pressure. Next, we consider the compliance of the upstream reservoir system. The eigenvalue equation (8) and the upstream and downstream pressures (9) and (10) now reduce to

$$\tan \phi L = -\alpha \lambda_u \phi, \tag{22}$$

$$p_u(t) = \frac{Q}{S_s AL + S_u}\left[t + \frac{\mu S_s^2 AL^3}{3k(S_s AL + S_u)}\right] - \frac{2Q}{kA}\sum_{m=1}^{\infty} \frac{\exp\left(-\alpha \phi_m^2 t\right)}{\phi_m^2\left(\alpha\lambda_u + L + \alpha^2 \lambda_u^2 \phi_m^2 L\right)} \tag{23}$$

and

$$p_d(t) = \frac{Q}{S_s AL + S_u}\left[t - \frac{\mu S_s^2 AL^3 + 3\mu S_s S_u L^2}{6k(S_s AL + S_u)}\right] - \frac{2Q}{kA}\sum_{m=1}^{\infty} \frac{\exp\left(-\alpha \phi_m^2 t\right)/\cos(\phi_m L)}{\phi_m^2\left(\alpha\lambda_u + L + \alpha^2 \lambda_u^2 \phi_m^2 L\right)}. \tag{24}$$

Three pairs of theoretical curves for the upstream and downstream pressures calculated from equations (23) and (24), obtained by varying k, S_s and S_u in turn, keeping the other variables constant are plotted in Figures 4a, 4b, and 4c, respectively. The results can be summarized as follows. Firstly, the permeability k influences only the upstream pressure intercept or the differential pressure ΔP of the steady state, and not its slope (Figure 4a). A lower permeability causes a higher differential pressure (ΔP_1 is larger than ΔP_2 when k_1 is less than k_2 in Figure 4a). Secondly, the specific storage S_s affects both the slope and the differential pressure of the steady state (Figure 4b). A larger S_s leads to a lower slope and larger ΔP. If S_u is zero, S_s has no effect on ΔP according to equation (21). Thirdly, the effect of S_u on the fluid pressure behavior is similar to that of S_s on the slope, but opposite to the effect of S_s on ΔP (Figure 4c). A larger S_u causes both the slope and the differential pressure to decrease. Finally, we note that a much shorter time is taken to reach the steady state than for the same rock specimen when the downstream end is open, as seen by comparing the examples in Figure 4c with those in Figure 2b. For $S_u = 6 \times 10^{-8}$ m^3/MPa, it takes less than 12 hours for $S_d = 0$, but about 100 hours for $S_d = \infty$. This is a second practical advantage of this test configuration, i.e., its relatively short duration makes it particularly useful for low-porosity rocks.

[19] We now show how to determine the hydraulic properties of a rock specimen from the time-based record of the fluid pressures at the upstream and/or downstream reservoirs in the case $S_u \neq 0$. If the time is large enough for

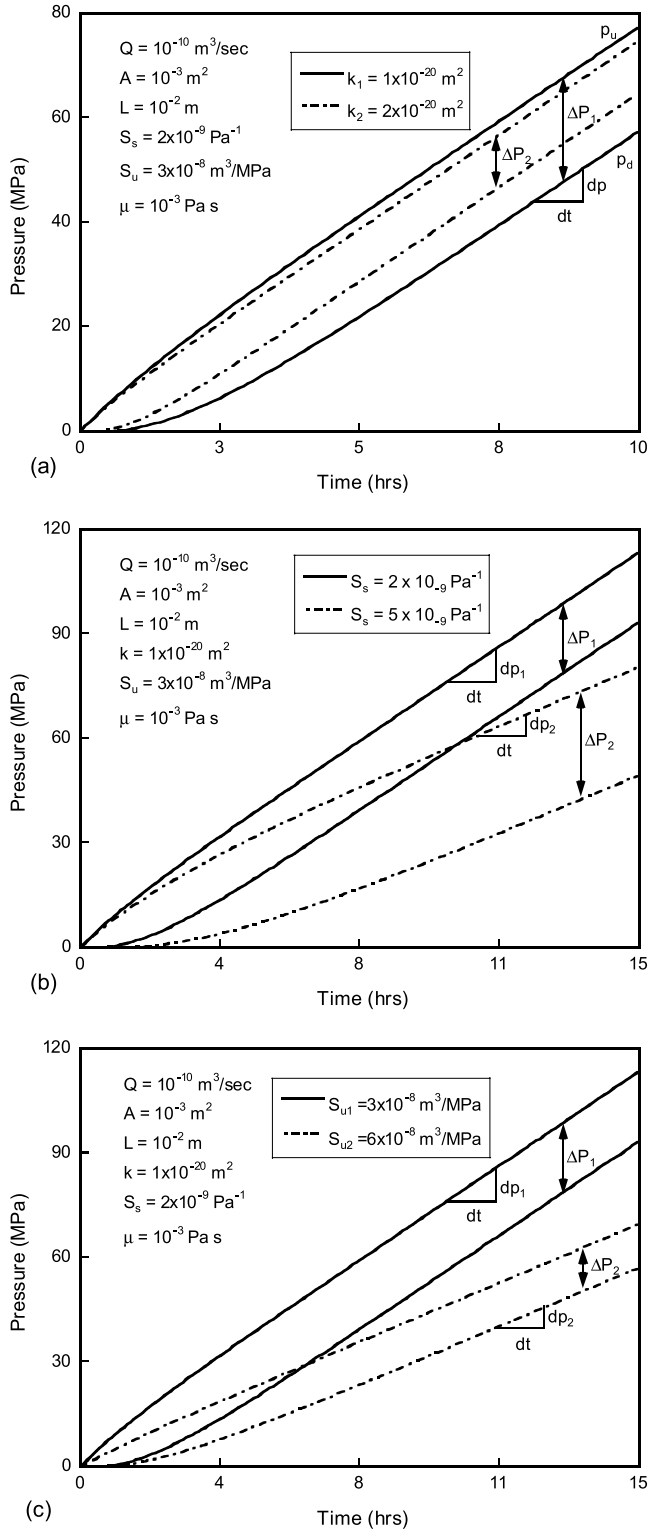

Figure 4. Theoretical pressures as a function of time for (a) different permeability, (b) different specific storage, and (c) different the compressive storage of the upstream reservoir showing the effects of each parameter on the characteristics of the pressure curves. Details are described in text.

the exponential term in the pressures (23) and (24) to be negligible, only the steady state remains as a linear function. The constant slope of this steady state is

$$\frac{dp_u}{dt} = \frac{dp_d}{dt} = \frac{Q}{S_s AL + S_u}. \tag{25}$$

This slope can be determined from the time-based record of the fluid pressure at the upstream and/or the downstream reservoirs, as shown in Figure 4. The differential pressure ΔP between the upstream and the downstream is

$$\Delta P = p_u - p_d = \frac{\mu Q S_s L^2}{2k(S_s AL + S_u)}. \tag{26}$$

In this scenario, ΔP is no longer independent of S_s. However, if the compressive storage S_u of the upstream reservoir is known independently, S_s can be obtained uniquely from the slope of the steady state using equation (25) when the other parameters (Q, A, L, and S_u) are known. Once S_s is determined, k can be calculated from the asymptotic differential pressure ΔP using equation (26) for a known fluid viscosity μ. Again, if it is not possible to record the downstream pressure, the permeability can be determined from the intercept of the linear asymptotic upstream pressure ($t = 0$) as

$$P_u^{\text{int}} = \frac{\mu Q S_s^2 AL^3}{3k(S_s AL + S_u)^2}. \tag{27}$$

This equation for the intercept is a little more complicated than equation (26) for the differential pressure, so that there is more chance for inaccuracy in the calculation of k, particularly from propagation of errors in S_u and S_s. The differential pressure ΔP is a direct measure, rather than an estimate based on the extrapolation of the slope as shown in Figure 3. Thus the measurement of ΔP is recommended for obtaining a more accurate value of the permeability if the measurement of the downstream pressure is possible. However, this requires a "zero-volume" pressure transducer endplug [e.g., *Green and Wang*, 1986; *Hart and Wang*, 2001] that may introduce its own uncertainties into the measurement (random and/or systematic), as discussed in the next section.

3.3. General Boundary Conditions

[20] There is a technical reason to consider that the downstream reservoir has a finite value of the compressive storage S_d. It may not be possible to use a completely rigid pressure transducer to read the fluid pressure at the downstream because the deflection of the diaphragm of the pressure transducer induces a small but finite additional storage on the downstream side. Such a small S_d may be negligible for some rock specimens with a large specific storage. However, if the specific storage of the specimen is small, neglecting S_d may lead to a serious inaccuracy in the calculation of the hydraulic properties of specimen if the equations in the previous section for the downstream pressure are used. Of course, the upstream pressure record is enough to determine both the permeability and the specific storage on its own upon using equations (25) and (27). For a more accurate calculation of the hydraulic properties, however, it is advisable to record the downstream pressure too.

[21] As shown by equation (7), the analytic solution of the general diffusion equation consists of two parts, the asymptotic (steady state) solution and the transient represented by the series solution. The second part decays exponentially with time and eventually becomes negligible as we showed above. For a large t, the asymptotic solution becomes dominant for the upstream and downstream pressures, so that equations (9) and (10) become in the case of a finite S_d

$$p_u(t) = \frac{Qt}{S_s AL + S_u + S_d} + \frac{\mu QL}{kA}\left(\frac{1}{3} + \frac{S_d}{S_s AL} + \frac{S_d^2}{S_s^2 A^2 L^2}\right) \cdot \left(1 + \frac{S_u + S_d}{S_s AL}\right)^{-2} \tag{28}$$

and

$$p_d(t) = \frac{Qt}{S_s AL + S_u + S_d} - \frac{\mu QL}{kA}\left(\frac{1}{6} + \frac{S_u + S_d}{2S_s AL} + \frac{S_u S_d}{S_s^2 A^2 L^2}\right) \cdot \left(1 + \frac{S_u + S_d}{S_s AL}\right)^{-2}. \tag{29}$$

These two pressures are linear functions of time. Again, the slopes of each pressure give the specific storage and the differential pressure yields the permeability if S_u and S_d are determined independently. The slope dp_u/dt and the differential pressure ΔP between p_u and p_d can be expressed as

$$\frac{dp_u}{dt} = \frac{Q}{S_s LA + S_u + S_d} \tag{30}$$

and

$$\Delta P = \frac{\mu QL}{kA}\left(\frac{1}{2} + \frac{S_d}{S_s AL}\right)\left(1 + \frac{S_u + S_d}{S_s AL}\right)^{-1}. \tag{31}$$

If reading the downstream pressure is not possible, we can compute the permeability from the intercept P_u^{int} of the upstream pressure using

$$P_u^{\text{int}} = \frac{\mu QL}{kA}\left(\frac{1}{3} + \frac{S_d}{S_s AL} + \frac{S_d^2}{S_s^2 A^2 L^2}\right)\left(1 + \frac{S_u + S_d}{S_s AL}\right)^{-2}. \tag{32}$$

In real tests, both the slope and intercept are determined based on the asymptotic part of test records. The slope is stable after the transients decay. Again, the intercept may possess inaccuracies because it is determined by the extrapolation of a line that may be established far from the origin. Thus a small change in the slope can cause a large difference in the intercept. Instead of using the intercept, we propose using the differential pressure ΔP between the two reservoirs where possible. We then are able to calculate the specific storage and the permeability using

$$S_s = \frac{Q - (S_u + S_d)dp/dt}{AL \cdot dp/dt} \tag{33}$$

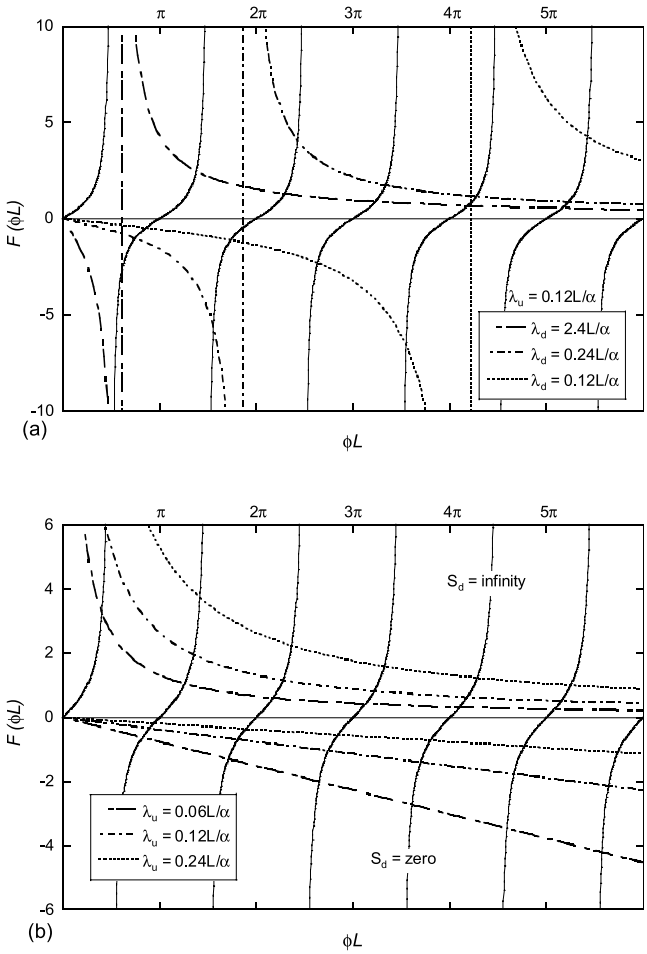

Figure 5. Plots of eigenvalue equation (8) showing periodic tangent functions and hyperbolic functions (a) for three different cases of the downstream compressive storage with a given value of the upstream compressive storage, and (b) for three examples of the upstream storage in two extreme cases of the downstream compressive storage. In both plots, ϕ_m can be obtained from each intersection point.

and

$$k = \mu L\left(\frac{Q - (S_u - S_d)dp/dt}{2A\Delta P}\right). \tag{34}$$

These equations are the most general for the case of a closed system with finite S_u, S_d and constant Q.

3.4. Analysis of the Transient

[22] Unlike the pulse transient method, our new method does not need the transient part of the fluid pressure variation to compute both the permeability and specific storage. The asymptotic (steady state) part dominates after the transient part decays, i.e., the importance of the transient part of our solution is related to the length of the experimental test. Of the transient terms, the first term ($m = 0$) is the most dominant term as time increases. The solution parameters are α and ϕ, both of which are positive, so that the exponential term decays to zero as t increases. α is a material parameter related to the permeability of the rock specimen and ϕ is a test system parameter determined from the eigenvalue equation (8).

[23] We plotted the eigenvalue equation (8) for a given value of λ_u and 3 different values of λ_d in Figure 5a, where the roots ϕ_m are the intersection points between the two functions, on the right hand and left hand sides of equation (8). These roots could be found by a simple numerical method such as the bisection algorithm [*Burden and Faires*, 1989]. As λ_d decreases, ϕ_m increases for a given value of m. Now as ϕL increases, the exponential transient term decays more rapidly to zero. Two special cases for λ_d are shown in Figure 5b, where the lower half is for the case $\lambda_d = 0$ and the upper half for $\lambda_d = \infty$. In both cases, as the upstream compressibility storage decreases, $\phi_m L$ for fixed m increases, so that the transient part decays more rapidly. This analysis demonstrates that we need to minimize the compressive storages of both the upstream and downstream reservoirs to minimize the test time. Also a larger stiffness of the test system yields a more accurate result.

Table 1. Basic Physical Parameters of Westerly Granite

Parameter	Value
Wet unit weight, kN/m^3	25.76
Dry unit weight, kN/m^3	25.71
Porosity, %	0.48

4. Application to Laboratory Measurements

4.1. Test Arrangement

[24] Our proposed method has been applied to the measurement of the permeability and the specific storage of cored rock specimens. The major purpose of this experimental work is limited to illustrating the accuracy and efficiency of our new laboratory measurement method. For a laboratory demonstration, we selected Westerly granite. The basic physical parameters of the rock type are listed in Table 1. We prepared two core specimens, 38 mm in diameter and 40 mm in length. The end faces of each specimen were machined to a smooth finish and to be parallel to each other. Both samples were immersed in degassed-deionized-distilled water and submitted to a vacuum for 24 hours at room temperature to let them saturate. The specimen assembly was inserted into a pressure vessel for the application of a confining pressure (Figure 6). Confining pressure was kept constant throughout each test cycle at 35 MPa. Porous steel spacers were placed on both sides of the rock specimen to distribute the fluid flux evenly throughout the cross section of the

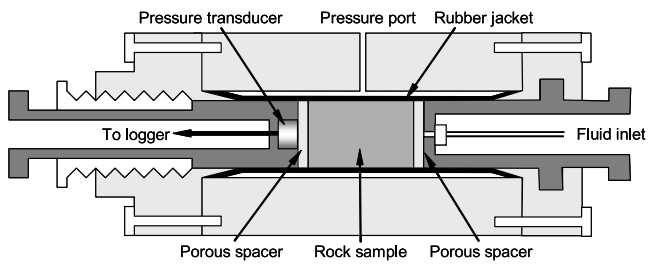

Figure 6. Section diagram of the triaxial pressure vessel with a specimen assembly.

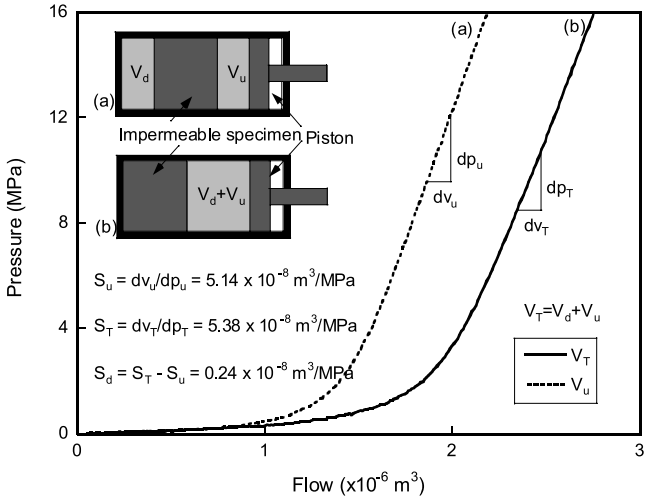

Figure 7. Schematic drawing of the test arrangement for determining the compressive storage of our test system and examples of calibration records for the upstream compressive storage (curve a) and the total (upstream and downstream reservoirs) compressive storage (curve b). The compressive storage of the downstream reservoir can be obtained by subtracting the upstream compressive storage from the total compressive storage. The examples of the compressive storage are from the linear part of the record above 10 MPa.

sample. A pressure transducer endplug was placed at the downstream end of the sample. Fluid flow was induced through the sample, as shown schematically in Figure 1, by connecting the upstream endplug through stainless steel high pressure tubing to a pump filled with degassed deionized water. The pump used for these experiments was a Hydratron piston pump, in which a hardened piston is forced through a Teflon seal pack into a closed 70 cm^3 stainless steel barrel by a stepper-motor-driven actuator nut. The upstream pressure was monitored using a pressure transducer attached to the line between the pump and the rock specimen. With the above experimental arrangement, the upstream volume is controlled by the initial position of the piston in the pump barrel, and upstream pressure is raised by advancing the piston slowly into its barrel at constant speed after all filling valves have been closed. The fluid system thus corresponds exactly with the schematic of Figure 1, with the exception that the upstream volume of the pump barrel is connected to the sample face through steel tubing. Using a stepper motor driver has the advantage of accurate piston stroke control, but the disadvantage of a limited range of available piston speeds.

4.2. System Compliance

[25] Before rock tests, we calibrated our test system in terms of the compressive storages of the upstream and downstream reservoirs as given by equations (1) and (2). The calibration arrangement was the same as for the rock tests shown in Figure 6, but an impermeable steel specimen was used instead of rock samples, as depicted in Figure 7. The upstream compressive storage S_u can be determined simply by replacing the rock specimen with the impermeable substance as shown in Figure 7 (curve a). In this case, $q(t) = 0$ in equation (1), leading to

$$Q = S_u \frac{dp_u}{dt}, \tag{35}$$

where Q is the flow rate generated by the pump and dp_u/dt the rate of pressure increase due to the piston stroke into an enclosed space. Thus S_u can be simply obtained from equation (35). In this problem, it was impossible to measure the compressive storage of the downstream reservoir S_d because it was not directly connected to the pump system. However, S_d can be determined by subtracting the upstream compressive storage S_u from the total compressive storage S_T, which in turn can be obtained from the total reservoir volume V_T of the upstream and downstream reservoirs, V_u and V_d. A schematic diagram of the test setup for measuring the total compressive storage S_T and the resultant pressure record is depicted in Figure 7 (curve b). S_T can be found from

$$Q = S_T \frac{dp_T}{dt}, \tag{36}$$

where dp_T/dt is the pressurization rate in the total reservoir volume.

[26] An example of a record in terms of the fluid pressure for the total volume and the upstream reservoir versus the flow generated by the piston movement, respectively, is shown in Figure 7. The compressive storage of the upstream reservoir can be determined from the inverse slope of the curve. The compressive storage of the downstream reservoir can be obtained from the difference between the total and the upstream compressive storages. Because we used two porous steel frits on both sides of the steel specimen, the compressive storage of the porous disks was incorporated in our calibration. The recorded curves are clearly linear over 8 MPa. The nonlinear behavior under 8 MPa results probably from the deformation of rubber O-ring used for sealing around the piston. The pore pressure was kept higher than 8 MPa during our tests in order that the compressive storages of the test system might be constant in each cycle of tests. We could not test in the nonlinear zone because the system compliance changes too rapidly as the fluid pressure increases.

[27] Even in the relatively linear zones, the curve is not perfectly linear because the compressive storage is a function of the fluid pressure [*Mok et al.*, 2002]. Thus we divided the curve into several segments each with a more constant value of the compressive storage and then each cycle of test was completed within each linear segment with a single value of compressive storage. The compressive storage is a function of the original volume of reservoir, i.e., the bigger the storage, the higher the induced compressive storage. This means that the compressive storage is dependent upon the position of the piston. We kept the starting position of piston consistent in the calibration and in every test to minimize any difference in the system compliance between the calibration and the test. Also by changing the starting position of the piston, we were able to test a

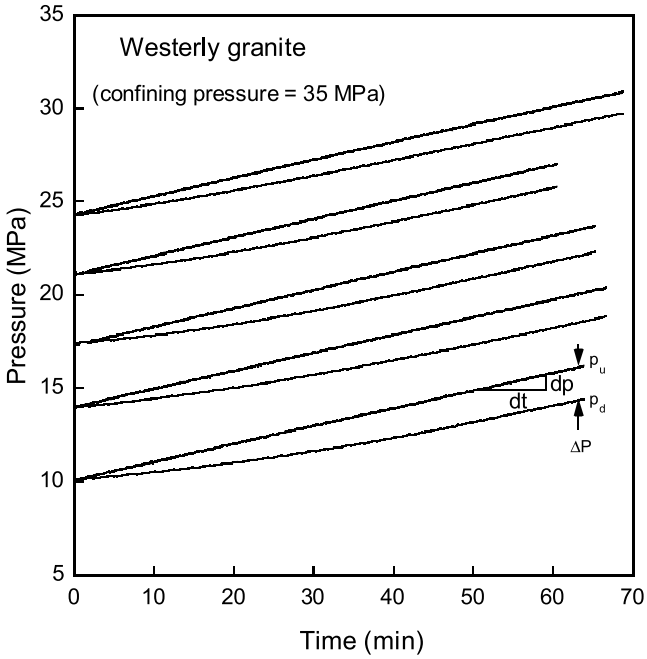

Figure 8. An example of test record for Westerly granite. Fluid injection with a constant flow rate was conducted at several different levels of pore pressure. Injection was continued until a linear segment of pressure increase at both reservoirs was clearly shown after the transient stage. Note that the differential pressure ΔP decreases with increasing pore pressure.

specimen with different compressive storages in order to validate the consistency of rock properties under different system compliances.

4.3. Test Results

[28] An example of the time-based record of fluid pressure variation at the upstream and downstream reservoirs arising from constant-rate flow injection is given in Figure 8. Fluid injection with a constant flow rate was conducted at several different levels of pore pressure at a constant confining pressure of 35 MPa. At the beginning of each cycle, the pressures in both reservoirs are in equilibrium at a certain level. In agreement with the theoretical analysis mentioned above, the upstream pressure increases immediately after generating flow at a decreasing rate during the initial transient phase, while the downstream pressure reacts tardily at an increasing rate. Eventually both rates become identical and keep a constant value, so that both curves become linear and parallel exactly as predicted by the theory. The transient for the upstream pressure is not clearly curved because the rock specimen is very tight. This was expected by the theoretical analysis (Figure 4).

[29] From each test record, we determined the slope (dp/dt) using a linear regression method and the average differential pressure (ΔP) of the stabilized curves, as shown in Figure 8. We were able to calculate the specific storage S_s and the permeability k of each specimen using equations (33) and (34), respectively. The result is plotted in the form of the hydraulic properties as a function of effective stress, which is the differential pressure between the confining and pore pressures (Figure 9). The specific storage S_s decreases with increasing effective pressure. On the basis of our results, we infer that the rock mass becomes stiffer as the effective pressure increases so that the pore pressure decreases (Figure 9a). The permeability decreases with average effective pressure, probably due to the opening of cracks and pores. As shown in Figure 9b, our data are consistent with those obtained from the pulse transient method [*Brace et al.*, 1968; *Lin*, 1982]. This result is consistent with previous studies concluding that k decreases with increasing effective stress [*Brace et al.*, 1968; *Trimmer et al.*, 1980; *Lin*, 1982; *Kwon et al.*, 2001].

[30] We also tested the two rock specimens in different system conditions. For example, S_u can be easily adjusted by changing the position of the piston. This allows several tests for one specimen with different system parameters without changing the test setup. The result from several tests is much more convincing than that from a single test, so we conducted the hydraulic tests of Westerly granite samples under various conditions in terms of the compressive storage S_u and the pumping rate Q. As listed in Table 2, the consistency of the

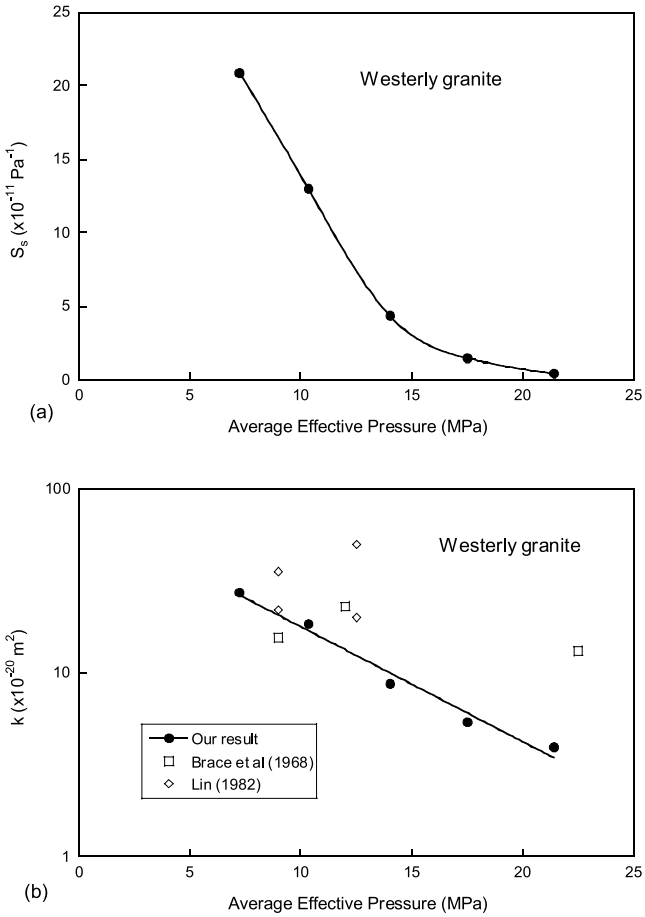

Figure 9. (a) Specific storage and (b) permeability as a function of effective circumferential stress in Westerly granite. Also shown is that our result is consistent with previous reference data obtained from the pulse transient method by *Brace et al.* [1968] and *Lin* [1982].

Table 2. Hydraulic Test Results in Varied Test Conditions in Two Samples of Westerly Granite

Test	S_u, m^3/Mpa	S_d, m^3/MPa	Q, m^3/sec	dp/dt, MPa/s	ΔP, MPa	S_s, Pa^{-1}	k, m^2
			Sample WG1				
WG1F07	1.7×10^{-8}	2×10^{-11}	6.82×10^{-10}	0.0293	10.6	1.5×10^{-10}	3.4×10^{-19}
WG1R07	4.1×10^{-8}	2×10^{-11}	6.82×10^{-10}	0.0148	4.09	1.3×10^{-10}	3.7×10^{-19}
WG1F10	1.0×10^{-8}	2×10^{-11}	9.74×10^{-10}	0.0380	13.4	1.6×10^{-10}	3.7×10^{-19}
WG1R10	3.7×10^{-8}	2×10^{-11}	9.74×10^{-10}	0.0221	9.45	1.8×10^{-10}	3.3×10^{-19}
Average						1.6×10^{-10}	3.5×10^{-19}
Standard deviation						2.0×10^{-11}	2.1×10^{-20}
			Sample WG2				
WG2R07	4.3×10^{-8}	2×10^{-11}	6.82×10^{-10}	0.0147	3.26	9.5×10^{-11}	3.5×10^{-19}
WG2R10	4.3×10^{-8}	2×10^{-11}	9.74×10^{-10}	0.0212	3.98	8.4×10^{-11}	3.6×10^{-19}
WG2F10	1.9×10^{-8}	2×10^{-11}	9.74×10^{-10}	0.0430	8.16	8.9×10^{-11}	3.8×10^{-19}
Average						8.9×10^{-11}	3.6×10^{-19}
Standard deviation						5.4×10^{-12}	1.7×10^{-20}

calculated hydraulic properties for different test conditions suggests that our method is reasonably reliable for laboratory measurements.

5. Discussion

[31] The solution of the partial differential equation with given initial-boundary conditions describes the evolution of the fluid pressure as a function of time and position. This evolution also depends on the material and system parameters. The interesting hydraulic parameters, e.g., k and S_s, of rock specimens can be determined from the measurement of the variation of the fluid pressure with time at a given position, on knowing the test system parameters. In order to solve the differential equation, we need appropriate initial-boundary conditions which can be controlled in a laboratory test arrangement. Different initial-boundary conditions correspond to different experimental techniques for measuring the hydraulic properties [e.g., *Brace et al.*, 1968; *Hsieh et al.*, 1981; *Morin and Olsen*, 1987; *Kranz et al.*, 1990; *Esaki et al.*, 1996]. All techniques are limited in accuracy and utility by their assumptions and system conditions [*Kranz et al.*, 1990].

[32] Here we first derived an analytic solution of the general diffusion equation with new initial-boundary conditions. On the basis of the analytical solution, we developed a new experimental technique which can simultaneously calculate the hydraulic permeability and the specific storage of a rock sample directly from the record of the upstream and downstream fluid pressures induced by constant-rate flow pumping. As we showed in theoretical and practical examples, the most important finding is the simplicity of both the inversion for the two hydraulic properties, k and S_s, and of the test setup and procedure. The computation process is quite straightforward. Unlike the pulse transient method [*Brace et al.*, 1968; *Lin*, 1982; *Zeynaly-Andabily and Rahman*, 1995] or the previous flow pump permeability test [*Morin and Olsen*, 1987; *Esaki et al.*, 1996], no tedious history curve-matching algorithm is required to obtain the hydraulic parameters.

[33] Another merit of our method is that it takes a relatively short time to conduct a complete test cycle. For example, it took a cycle of test about an hour for Westerly granite (Figure 8) in our test system. According to equation (31), the differential pressure ΔP can be controlled with the speed of piston (the pumping rate Q) and the test system compliance S_u and S_d. A good control of ΔP is important because the permeability is a function of the pore pressure for a given confining pressure or effective stress [*Wu and Pruess*, 2000; *Liang et al.*, 2001]. With a large ΔP, it is hard to examine the variation of the permeability as a function of the effective stress because the effective stress varies along the specimen. By decreasing Q and increasing S_u and S_d, we could test at different pore pressure levels for a given confining pressure.

6. Conclusions

[34] We described in this paper the one-dimensional fluid diffusion along a cored rock sample induced by constant-rate flow pumping using an analytic solution derived from the general diffusion equation with appropriate boundary and initial conditions for a rock specimen placed between two reservoirs. On the basis of the analysis of the analytic solution, we developed a new and relatively straightforward graphical technique for determining the specific storage and the permeability of a cored rock sample from the record of the upstream or/and downstream fluid pressures generated by constant-rate flow pumping. We tested our new method with two cored samples of Westerly granite. Simply computed values of the specific storage and the permeability of each specimen were consistent with those from the literature. In addition to the simplicity, we also found many other merits of our method to evaluate the hydraulic properties of rocks, such as reliability, economy of time and flexibility of system parameters for testing in different conditions.

Appendix A

[35] A brief description of how to solve the general diffusion equation (3) is given here. Taking Laplace transforms of equation (3) yields

$$\int_0^\infty e^{-st} \frac{\partial^2 p}{\partial x^2} dt - \frac{1}{\alpha} \int_0^\infty e^{-st} \frac{\partial p}{\partial t} dt = 0. \tag{A1}$$

Equation (A1) with the initial condition, equation (4), can then be expressed in the form of an ordinary differential equation

$$\frac{d^2 \overline{p}}{dx^2} - q^2 \overline{p} = 0 \quad \text{with} \quad q^2 = \frac{s}{\alpha}, \tag{A2}$$

where $\overline{p}$ is the Laplace transform of p. The general solution of equation (A2) is

$$\overline{p} = C_1 e^{qx} + C_2 e^{-qx}. \tag{A3}$$

Taking Laplace transforms of the boundary conditions, equations (5) and (6), we can determine C_1 and C_2 in equation (A3), so that the equation (A3) becomes

$$\overline{p} = \frac{F}{s} \frac{q\cosh qx + \lambda_d s \sinh qx}{(q^2 + \lambda_u\lambda_d s^2)\sinh qL + sq(\lambda_u + \lambda_d)\cosh qL}, \tag{A4}$$

where $\lambda_u = S_u/KA$, $\lambda_d = S_d/KA$, $F = Q/KA$, and $K = k/\mu$.

[36] The inversion of the Laplace transform (A4) is obtained by the usual inverse formula

$$p = \frac{1}{2\pi i}\int_C e^{st}\overline{p}\,ds, \tag{A5}$$

where C is the straight contour from $\gamma - i\infty$ to $\gamma + i\infty$ and γ lies to the right of all singularities of $\overline{p}$. The contour integral (A5) can then be evaluated by completing the contour to the left and summing residues. Now $e^{st}\overline{p}$ has a double pole at $s = 0$. If we take the first two terms in the Taylor series for sinh x and cosh x, $\overline{p}$ becomes

$$\overline{p} = \frac{1}{s^2}\frac{F + F\left(t + \frac{x^2}{2\alpha} + \lambda_d x\right)s + F\left(\frac{x^2}{2\alpha}t + \lambda_d x t + \frac{\lambda_d x^3}{6\alpha}\right)s^2 + \frac{\lambda_d x^3}{6\alpha}ts^3}{\left(\frac{L}{\alpha} + \lambda_u + \lambda_d\right) + \left(\frac{L^3}{6\alpha^2} + \lambda_u\lambda_d L + \frac{\lambda_u + \lambda_d}{2\alpha}L^2\right)s + \left(\frac{\lambda_u\lambda_d L^3}{6\alpha}\right)s^2} + \cdots. \tag{A6}$$

Now the residue at a pole of order m at $z = a$ of a function $f(z)$ is

$$\operatorname*{Res}_{z=a} f(z) = \frac{1}{(m-1)!}\lim_{z\to a}\left\{\frac{d^{m-1}}{dz^{m-1}}\left[(z-a)^m f(z)\right]\right\} \tag{A7}$$

Therefore as $m = 2$, the residue of $e^{st}\overline{p}$ at $s = 0$ is

$$\operatorname*{Res}_{s=0}(e^{st}\overline{p}) = \lim_{s\to 0}\frac{d}{ds}s^2(1+st)\overline{p}(s) = \frac{F}{\beta}t + \frac{F}{2\alpha\beta}\left[x^2 + 2\alpha\lambda_d x\right] - \frac{F}{6\alpha^2\beta^2}\left[L^3 + 3\alpha(\lambda_u + \lambda_d)L^2 + 6\alpha^2\lambda_u\lambda_d L\right] \tag{A8}$$

on expanding to the first two terms in a Taylor series, where

$$\beta = \left(\frac{L}{\alpha} + \lambda_u + \lambda_d\right).$$

The $\overline{p}$ also has simple poles when the denominator in equation (A4) vanishes, i.e., when

$$\left(q^2 + \lambda_u\lambda_d s^2\right)\sinh qL + sq(\lambda_u + \lambda_d)\cosh qL = 0. \tag{A9}$$

This equation has pure imaginary solutions for q, so that

$$q = i\phi \quad \text{and} \quad q^2 = -\phi^2, \tag{A10}$$

where ϕ is a real number. Then from equation (A2)

$$s = -\alpha\phi^2 \quad \text{and} \quad q^2 = \frac{s}{\alpha}, \tag{A11}$$

so that s is always negative.

[37] The transcendental equation (A9) can be rewritten by substituting equations (A11) and (A12):

$$\tan\phi L = \frac{\alpha\phi(\lambda_u + \lambda_d)}{\lambda_u\lambda_d\alpha^2\phi^2 - 1}. \tag{A12}$$

The simple poles are then determined by the roots ϕ_m of this equation. Now $e^{st}\overline{p}$ is of the form $N(s)/D(s)$. For a simple pole at $s = s_m$, the residue is given by

$$\operatorname*{Re}_{s=s_m} s e^{st}\overline{p} = \frac{N(s_m)}{D'(s_m)} = \frac{-2F\exp\left(-\alpha\phi_m^2 t\right)(\cos\phi_m x - \alpha\lambda_d\phi_m\sin\phi_m x)}{\phi_m a\sin\phi_m L + \phi_m^2 b\cos\phi_m L}, \tag{A13}$$

where $a = 3 - 5\lambda_u\lambda_d\alpha^2\phi_m^2 - \alpha L(\lambda_u + \lambda_d)\phi_m^2$ and $b = L + 4\alpha(\lambda_u + \lambda_d) - \lambda_u\lambda_d\alpha^2 L\phi_m^2$. The complete analytical solution of the diffusion equation is then

$$p = \operatorname{Re}s(0) + \sum_{m=1}^{\infty}\operatorname{Re}s(s_m),$$

so that

$$p(x,t) = \frac{F}{\beta}t + \frac{F}{2\alpha\beta}\left[x^2 + 2\alpha\lambda_d x\right] - \frac{F}{6\alpha^2\beta^2}\left[L^3 + 6\alpha^2\lambda_u\lambda_d L + 3\alpha L^2(\lambda_u + \lambda_d)\right] - 2F\sum_{m=1}^{\infty}\frac{\exp\left(-\alpha\phi_m^2 t\right)(\cos\phi_m x - \alpha\lambda_d\phi_m\sin\phi_m x)}{\phi_m a\sin\phi_m L + \phi_m^2 b\cos\phi_m L}. \tag{A14}$$

[38] **Acknowledgments.** This research project (DGLab - Corinth) was funded by the specific program on "Energy, Environment and Sustainable Development" (EESD). Project reference EU: EVR1-2000-40005.

References

Biot, M. A. (1941), General theory of three-dimensional consolidation, *J. Appl. Phys.*, *12*, 155–164.

Brace, W. F., J. B. Walsh, and W. T. Frangos (1968), Permeability of granite under high pressure, *J. Geophys. Res.*, *73*, 2225–2236.

Burden, R. L., and J. D. Faires (1989), *Numerical Analysis*, 4th ed., 729 pp., PWS-KENT, Boston.

Carslaw, H. S., and J. C. Jaeger (1959), *Conduction of Heat in Solids*, 510 pp., Oxford Univ. Press, New York.

Detournay, E., and A. H.-D. Cheng (1988), Poroelastic response of a borehole in a non-hydrostatic stress field, *Int. J. Rock Mech. Min. Sci. Geomech. Abstr.*, *25*, 171–182.

Esaki, T., M. Zhang, A. Takeshita, and Y. Mitani (1996), Rigorous theoretical analysis of a flow pump permeability test, *Geotech. Test. J.*, *19*, 241–246.

Fournier, R. O. (1996), Compressive and tensile failure at high fluid pressure where preexisting fracture have cohesive strength, with application to the San Andreas fault, *J. Geophys. Res.*, *101*, 25,499–25,509.

Green, D. H., and H. F. Wang (1986), Fluid pressure response to undrained compression in saturated sedimentary rock, *Geophysics*, *51*, 948–956.

Hart, D. J., and H. F. Wang (2001), A single test method for determination of poroelastic constants and flow parameters in rocks with low hydraulic conductivities, *Int. J. Rock Mech. Min. Sci.*, *38*, 577–583.

Hsieh, P. A., J. V. Tracy, C. E. Neuzil, J. D. Bredehoeft, and S. E. Silliman (1981), A transient laboratory method for determining the hydraulic properties of tight rocks-I. Theory, *Int. J. Rock Mech. Min. Sci. Geomech. Abstr.*, *18*, 245–252.

Johnson, A. G., R. L. Kovach, and A. Nur (1973), Pore pressure changes during creep events on the San Andreas fault, *J. Geophys. Res.*, *78*, 851–857.

Kranz, R. L., J. S. Saltzman, and J. D. Blacic (1990), Hydraulic diffusivity measurements on laboratory rock samples using an oscillating pore pressure method, *Int. J. Rock Mech. Min. Sci. Geomech. Abstr.*, *27*, 345–352.

Kwon, O., A. K. Kronenberg, and A. F. Gangi (2001), Permeability of Wilcox shale and its effective pressure law, *J. Geophys. Res.*, *106*, 19,339–19,353.

Liang, Y., J. D. Price, D. A. Wark, and E. B. Watson (2001), Nonlinear pressure diffusion in a porous medium: Approximate solutions with applications to permeability measurements using transient pulse decay method, *J. Geophys. Res.*, *106*, 529–535.

Lin, C., G. Pirie, and D. A. Trimmer (1986), Low permeability rocks: Laboratory measurements and three-dimensional microstructural analysis, *J. Geophys. Res.*, *91*, 2173–2181.

Lin, W. (1982), Parametric analysis of the transient method of measuring permeability, *J. Geophys. Res.*, *87*, 1055–1060.

Mok, U., Y. Bernabé, and B. Evans (2002), Permeability, porosity and pore geometry of chemically altered porous silica glass, *J. Geophys. Res.*, *107*(B1), 2015, doi:10.1029/2001JB000247.

Morin, R. H., and H. W. Olsen (1987), Theoretical analysis of the transient pressure response from a constant flow rate hydraulic conductivity test, *Water Resour. Res.*, *23*, 1461–1470.

Mortensen, C. E., R. C. Lee, and R. O. Burford (1977), Observations of creep-related tilt, strain, and water-level changes on the central San Andreas fault, *Bull. Seismol. Soc. Am.*, *67*, 641–649.

Neuzil, C. E., C. Cooley, S. E. Silliman, J. D. Bredehoeft, and P. A. Hsieh (1981), A transient laboratory method for determining the hydraulic properties of tight rocks-II. Application, *Int. J. Rock Mech. Min. Sci. Geomech. Abstr.*, *18*, 253–258.

Olsen, H. W., R. W. Nichols, and T. L. Rice (1985), Low gradient permeability measurements in a triaxial system, *Geotechnique*, *35*, 145–157.

Rice, J. R., and M. P. Cleary (1976), Some basic stress diffusion solutions for fluid-saturated elastic porous media with compressible constituents, *Rev. Geophys.*, *14*, 227–241.

Roeloffs, E. A., S. S. Burford, F. S. Riley, and A. W. Records (1989), Hydrologic effects on water level changes associated with episodic fault creep near Parkfield, California, *J. Geophys. Res.*, *94*, 12,387–12,402.

Roxburgh, I. S. (1987), *Geology of High-Level Nuclear Waste Disposal*, 228 pp., Chapman and Hall, New York.

Savage, D., (Ed.) (1995), *The Scientific and Regulatory Basis for the Geological Disposal of Radioactive Waste*, 437 pp., John Wiley, Hoboken, N. J.

Simpson, G. (2001), Influence of compression-induced fluid pressures on rock strength in the brittle crust, *J. Geophys. Res.*, *106*, 19,465–19,478.

Simpson, G., Y. Guéguen, and F. Schneider (2001), Permeability enhancement due to microcrack dilatancy in the damage regime, *J. Geophys. Res.*, *106*, 3999–4016.

Trimmer, D., B. Bonner, C. Heard, and A. Duba (1980), Effect of pressure and stress on water transport in intact and fractured gabbro and granite, *J. Geophys. Res.*, *85*, 7059–7071.

Wong, T.-F., and R. Biegel (1985), Effects of pressure on the micromechanics of faulting in San Marcos gabbro, *J. Struct. Geol.*, *7*, 737–749.

Wu, Y.-S., and K. Pruess (2000), Integral solutions for transient fluid flow through a porous medium with pressure-dependent permeability, *Int. J. Rock Mech. Min.*, *37*, 51–61.

Zeynaly-Andabily, E. M., and S. S. Rahman (1995), Measurement of permeability of tight rocks, *Meas. Sci. Technol.*, *6*, 1519–1527.

Zoback, M. D., and J. D. Byerlee (1975), The effect of microcrack dilatancy on the permeability of Westerly granite, *J. Geophys. Res.*, *80*, 752–755.

S. C. Elphick, I. G. Main, B. T. Ngwenya, and N. W. Odling, School of Geosciences, University of Edinburgh, Edinburgh EH9 3JW, UK. (stephen.elphick@glg.ed.ac.uk)

N. F. Smyth, School of Mathematics, University of Edinburgh, Edinburgh EH9 3JZ, UK. (n.smyth@ed.ac.uk)

I. Song, Institute for Geology, Mineralogy, and Geophysics, Ruhr-University Bochum, D-44780 Bochum, Germany. (insun.song@ruhr-uni-bochum.de)